result of a difference in work function with the underlying substrate (*5*). This shifts k_F to $k_F \pm \delta k$ with $\delta k = \delta E/\hbar v_F$, and λ_F thus becomes $(2\pi)/(k_F \pm \delta k) = 0.69$ nm (+) or 0.79 nm (–). The experimentally observed wavelengths (Fig. 3B) correspond well to the theoretical values, confirming the predicted band structure with two linear bands crossing near E_F. This result provides quantitative evidence for our interpretation of the oscillations in dI/dV in terms of wave functions of discrete electron states.

A short metallic nanotube resembles the textbook model for a particle in a 1D box. For a discrete energy state with quantum number n, the corresponding wavelength $\lambda_n = 2L/n$. The observed wavelength is much smaller than the tube length, in accordance with the fact that the number of electrons within one nanotube band is large ($n \sim 10^2$). The wavelength will therefore vary only slightly ($\Delta\lambda_n = \lambda_n/n \sim 0.01$ nm) for adjacent discrete energy levels in one band.

The measurements reported here are technically challenging because they require a large series of reproducible *I-V* curves. Occasionally, we were able to resolve some of the spatial structure in the wave function at a length scale smaller than the Fermi wavelength (Fig. 4A). In this scan the peak spacing is nonequidistant, leading to an apparent pairing of peaks. This feature indicates that the wave function does not conform to a simple sinusoidal form. Recent calculations by Rubio *et al.* (*17*) indicate a nontrivial spatial variation of the nodes in the wave function of discrete electron states in the direction perpendicular to the tube axis (Fig. 4B). Line profiles can show either pairing or an equidistant peak spacing, depending on the exact position of the line scan. The observation of pairing confirms that the relevant period in the line scans is the distance between next-nearest-neighbor peaks.

Our experiments demonstrate that individual wave functions corresponding to the quantized energy levels in a short metallic nanotube can be resolved because of the large energy level splitting. The technique for recording the wave periodicity at different energy states provides a tool for further exploration of the dispersion relation in nanotubes. Future work should include similar experiments on nanotubes with various chiral angles. The methodology presented here also opens up the possibility of obtaining full 2D spatial maps of the electron wave functions in carbon nanotubes.

References and Notes

1. M. S. Dresselhaus, G. Dresselhaus, P. C. Eklund, *Science of Fullerenes and Carbon Nanotubes* (Academic Press, San Diego, CA, 1996).
2. M. Bockrath *et al.*, *Science* **275**, 1922 (1997).
3. S. J. Tans *et al.*, *Nature* **386**, 474 (1997).
4. M. F. Crommie, C. P. Lutz, D. M. Eigler, *Science* **262**, 218 (1993); *Nature* **363**, 424 (1993); Y. Hasegawa and Ph. Avouris, *Phys. Rev. Lett.* **71**, 1071 (1993).
5. J. W. G. Wildöer, L. C. Venema, A. G. Rinzler, R. E. Smalley, C. Dekker, *Nature* **391**, 59 (1998).
6. T. W. Odom, J.-L. Huang, P. Kim, C. M. Lieber, *ibid.*, p. 62.
7. J. W. Mintmire, B. I. Dunlap, C. T. White, *Phys. Rev. Lett.* **68**, 631 (1992); N. Hamada, S.-I. Sawada, A. Oshiyama, *ibid.*, p. 1579; R. Saito, M. Fujita, G. Dresselhaus, M. S. Dresselhaus, *Appl. Phys. Lett.* **60**, 2204 (1992).
8. A. Thess *et al.*, *Science* **273**, 483 (1996).
9. Exact identification of the lattice indices (*n,m*) [see (*1*)] of chiral nanotubes is quite difficult because both the nanotube diameter and the chiral angle between hexagon rows and the tube axis must be measured with high accuracy. The (*n,m*) indices are crucial for chiral tubes because a minor change in one of these determines whether the tube is a metal or a semiconductor. For armchair tubes, however, the situation is easier. The nonchiral structure with hexagon rows running parallel to the tube axis can be easily observed from the atomically resolved images, and a precise determination of the diameter is not essential because armchair tubes of all diameters are metallic.
10. J. W. G. Wildöer, A. J. A. van Roij, H. van Kempen, C. J. P. M. Harmans, *Rev. Sci. Instrum.* **65**, 2849 (1994). In our setup the lateral drift is almost negligible (typically <1 nm per hour) because the STM is cooled in a ^{4}He bath cryostat. Successive STM spectroscopy line scans therefore show identical results. Over a longer period, however, the tip may change position slightly as a result of residual drift or minor changes in the tip.
11. L. C. Venema *et al.*, *Appl. Phys. Lett.* **71**, 2629 (1997). After this cutting event, the tip was cleaned by applying voltage pulses above the gold substrate, far away from the tube. Linear *I-V* spectroscopy curves on clean areas of the gold substrate demonstrated that the tip was free of debris.
12. The applied voltage is in principle divided into a part that drops over the tunnel gap and a part that drops between the nanotube and the substrate. The ratio α between these voltages is determined by the capacitance ratio. Because the capacitance between nanotube and substrate is much larger than that between the nanotube and the STM tip, the voltage will drop almost entirely over the tunnel gap, and accordingly α has a value close to 1.
13. W. T. Scott, *The Physics of Electricity and Magnetism* (Wiley, New York, ed. 2, 1966), pp. 163–165.
14. L. P. Kouwenhoven *et al.*, in *Mesoscopic Electron Transport*, L. L. Sohn, G. Schön, L. P. Kouwenhoven, Eds. (Kluwer, Dordrecht, Netherlands, 1997), pp. 105–214.
15. Note that the exact voltages at which the peaks in *dI/dV* appear in Figs. 2 and 3A are different. This can be attributed to variations in the offset charge caused by trapping of charge in the environment of the tube, as is well known in Coulomb charging phenomena [see R. Wilkins and R. C. Jaclevic, *Phys. Rev. Lett.* **63**, 801 (1989); J. G. A. Dubois, E. N. G. Verheijen, J. W. Gerritsen, H. Van Kempen, *Phys. Rev. B* **48**, 11260 (1993)]. Variation of the offset charge may change the Coulomb gap and thus shift the exact voltage at which the discrete levels of the tube appear in the *I-V* measurements. In fact, switching of offset charges was observed in some of our line scans. This effect is irrelevant for the observations reported here, which are the periodic oscillations in the differential conductance of discrete energy levels.
16. The total wave function is in fact defined by the atomic lattice potential modulated with a standing wave profile resulting from the confinement in the length direction. Because the STM tip follows the atomic corrugation by scanning in constant-current mode at a high bias voltage, the lattice periodicity is largely compensated so that the standing waves can be resolved in the spectroscopy measurements for several discrete states at low bias.
17. A. Rubio, E. Artacho, P. Ordejon, P. D. Sanchez-Portal, D. J. Soler, in preparation.
18. We thank R. E. Smalley and co-workers for supplying the nanotube material and A. Rubio for sharing results before publication. Supported in part by the Dutch Foundation for Fundamental Research of Matter (FOM). L.P.K. is supported by the Royal Dutch Academy of Sciences and Art (KNAW).

1 September 1998; accepted 20 November 1998

DOAS Measurements of Tropospheric Bromine Oxide in Mid-Latitudes

Kai Hebestreit, Jochen Stutz,* David Rosen, Valery Matveiv, Mordechai Peleg, Menachem Luria, Ulrich Platt

Episodes of elevated bromine oxide (BrO) concentration are known to occur at high latitudes in the Arctic boundary layer and to lead to catalytic destruction of ozone at those latitudes; these events have not been observed at lower latitudes. With the use of differential optical absorption spectroscopy (DOAS), locally high BrO concentrations were observed at mid-latitudes at the Dead Sea, Israel, during spring 1997. Mixing ratios peaked daily at around 80 parts per trillion around noon and were correlated with low boundary-layer ozone mixing ratios.

Sudden boundary-layer ozone (O_3) depletion events during Arctic spring (*1, 2*) are likely caused by the presence of reactive halogen species, particularly BrO. Bromine or BrO (or other halogens) catalytically convert two ozone molecules to three oxygen molecules without a loss of the halogen (*3*). Although the chemical cycles destroying ozone are well understood, the source of the reactive bromine compounds remains unclear, but they are most likely formed by oxidation of sea salt halogenides (*4*). Bromine oxide has been observed by DOAS in several places in the Arctic (*5, 6*) and Antarctica (*7*). Satellite-

---

K. Hebestreit, J. Stutz, U. Platt, Institut für Umweltphysik, Ruprecht-Karls-Universität Heidelberg, Im Neuenheimer Feld 366, D-69120 Heidelberg, Germany. D. Rosen, V. Matveiv, M. Peleg, M. Luria, Environmental Science, School of Applied Science, Hebrew University, 91904 Jerusalem, Israel.

*To whom correspondence should be addressed. E-mail: stu@uphys1.uphys.uni-heidelberg.de

based studies (*8*, *9*) show that elevated boundary-layer BrO concentrations are a widespread phenomenon covering areas of several million square kilometers. Elevated boundary layer BrO that cannot be attributed to polar bromine release processes has not been found outside polar regions (*10–12*). Here, we present DOAS measurements showing that Br is released from salt pans at the Dead Sea, Israel.

The Dead Sea differs from the normal marine environment in that the salinity of Dead Sea water is higher, the Br/Cl ratio of its salt is higher than that of ocean salt (*13*), and there are extended salt pans in the Dead Sea valley (*14*). A field campaign was performed at the Dead Sea from 27 May to 25 June 1997. A van with the instruments was set up on the dam between the northern and southern parts of the Dead Sea (31°21′N, 35°37′E), 21 km north of the salt pans. Elevated concentrations of BrO were expected for southerly winds if the salt pans are indeed a source of bromine; other directions should yield background levels only.

Different in situ monitors detected SO_2, NO/NO_2, CO, O_3, and meteorological parameters. The Long-Path DOAS (LP-DOAS) (*15*) system measured mainly BrO; O_3 and NO_2 were also detected (*16*). DOAS (*17*) measures atmospheric trace gases by use of their specific narrow-band (<5 nm) ultraviolet–visible light absorption structure in the open atmosphere, separating trace gas absorption from broad-band molecule and aerosol extinction. It is sensitive to many molecular species because they have unique specific absorption structures. Calibration of the instrument is not necessary if the absorption cross section of the species to be measured is known (*18*).

Bromine oxide was detected on all days of the campaign. The highest optical density of the BrO absorption was 8.1×10^{-3} (Fig. 1), corresponding to a BrO concentration of 2.1 ($\pm$0.3) $\times 10^9$ molecules per cubic centimeter or 86 ± 10 ppt. This mixing ratio is a factor of 3 above those measured at polar regions and a factor of ~6 above those measured in the stratosphere (*19*).

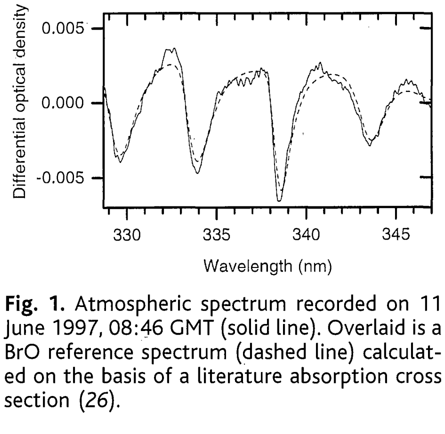

Fig. 1. Atmospheric spectrum recorded on 11 June 1997, 08:46 GMT (solid line). Overlaid is a BrO reference spectrum (dashed line) calculated on the basis of a literature absorption cross section (*26*).

The abundance of trace gases showed diurnal cycles that reflect the wind direction. Because the Dead Sea basin is oriented north-south, essentially only winds in these directions are observed. For northerly winds, no BrO was detected and O_3 mixing ratios were around 60 ppb. When the wind began to shift, for example at 3:00 GMT, a rise in BrO concentration was detected only several hours later (shaded band in Fig. 2). The measured wind speed and time lag can be used to identify the Br source. For an average wind speed of ~2.7 m/s in Fig. 2, the delay was 2.5 hours, and the source was located at a distance of ~24 km. This is approximately the distance of the salt pans. In this case, the decay of O_3 due to catalytic destruction by BrO was observed half an hour later, when its concentration suddenly dropped to the detection limit of 2 ppb within 15 min. This fast decay compared to the gradual BrO increase is because the DOAS instrument averages the BrO concentration over the light path of 3.75 km, whereas the ozone monitor samples in situ at the northern end of the DOAS light path. A rapid transport of an air mass with an elevated concentration is therefore observed as a smoothed signal in the DOAS. The transition time is due to the time the air needs to travel from the southern end of the light path to the in situ monitor. The BrO and O_3 concentrations returned to their original values when the wind changed back to northerly directions.

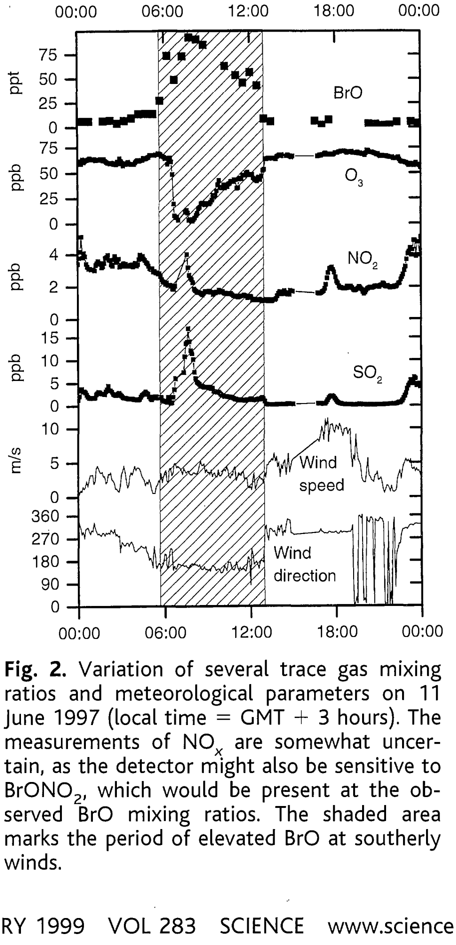

Fig. 2. Variation of several trace gas mixing ratios and meteorological parameters on 11 June 1997 (local time = GMT + 3 hours). The measurements of NO_x are somewhat uncertain, as the detector might also be sensitive to $BrONO_2$, which would be present at the observed BrO mixing ratios. The shaded area marks the period of elevated BrO at southerly winds.

On several occasions after the arrival of the BrO-enriched air, the concentrations of NO_x (= NO + NO_2) and SO_2, both typically emitted by industry or traffic, peaked. The sharpness of the peak indicates that an air mass was transported to the site without much dilution and therefore probably originated near the site. Because the region south of the site is not densely populated, the only plausible sources within 50 km are the Dead Sea Works, ~23 km south of the site, and a similar factory in Jordan, approximately the same distance away. Both factories manufacture various chemicals, including Br compounds, from the salt of the pans. Because the diurnal variation of the industrial emissions of NO_x and SO_2 and of the BrO concentrations are different, the factories can be ruled out as sources of the observed bromine. The time variation of the BrO signal also indicates that the bromine is released from an extended source rather than from a point source.

The repeating pattern of high BrO and depleted O_3 occurring only at southerly winds was observed every day (Fig. 3). The O_3 depletion connected to the release of bromine observed in the respective air masses can be explained by chemical processes taking place while the air travels from the salt pans to the site in about 2 to 3 hours. This time period is more than one order of magnitude shorter than the time for a complete O_3 depletion in the Arctic (*6*). Simple photochemical model calculations indicate that about 2 to 4 ppb of total bromine must be released to destroy a background level of 60 ppb of O_3 at the NO_x concentrations observed on 11 June. Whether the same bromine release processes as in the Arctic occur at the Dead Sea is not clear. It appears that the

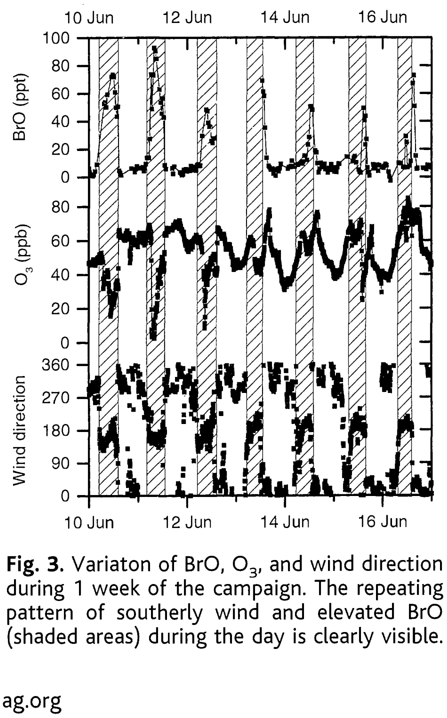

Fig. 3. Variaton of BrO, O_3, and wind direction during 1 week of the campaign. The repeating pattern of southerly wind and elevated BrO (shaded areas) during the day is clearly visible.

availability of salt surfaces enriched in bromide, as also observed on freezing seawater in the Arctic (*20*), is a prerequisite for bromine release.

Typical temperatures at the Dead Sea were 40°C, about 40 to 60 K higher than in polar spring. Apparently the presence of ice surfaces, as often assumed, is not necessary to release bromine. At the Dead Sea, Br is most likely released by a heterogeneous autocatalytic process from the surface of the salt pans. A release from the sea surface or from aerosols formed by breaking waves is unlikely, as no bromine was observed when the wind came from the north, traveling over the Dead Sea itself. Extended salt pans are found in many other locations; even if the Br/Cl ratio is not high, a release of Br appears possible. It is not clear whether bromine from salt pans influences ozone concentrations only locally or on larger scales.

References and Notes

1. J. W. Bottenheim, A. C. Gallant, K. A. Brice, *Geophys. Res. Lett.* **13**, 113 (1986).
2. S. J. Oltmanns and W. D. Komhyr, *J. Geophys. Res.* **91**, 5229 (1986).
3. R. P. Wayne *et al.*, *Atmos. Environ.* **29**, 2675 (1995).
4. Active bromine and active chlorine are most likely released (*11, 21*) from sea salt deposits or sea salt aerosol, which normally contain (by weight) 55.7% Cl^-, 0.19% Br^-, and 2×10^{-5} % I^-. Different heterogeneous release mechanisms have been proposed: (i) Reaction of nitrogen oxides (NO_2 or N_2O_5) with NaBr can form BrNO or $BrNO_2$, which are easily photolyzed, forming Br (*22*). (ii) The oxidation by OH of the HBr that has been released from aerosols by acidification through H_2SO_4 or HNO_3 is probably too slow to be important. (iii) An autocatalytic process may be important in which HOBr adsorbed on an acidic salt surface undergoes several reactions involving Br^- (*21, 23, 24*). The Br_2 formed in these reactions is released into the gas phase and can be photolyzed and converted into two HOBr molecules. If <50% of the oxidized bromine is lost from the autocatalytic cycle, an effective release process will take place. This mechanism is suspected to occur on sea ice surfaces or in aerosol during Arctic spring (or both). Bromine atoms can also be formed by photolysis of alkyl bromides, such as CH_3Br, emitted from algae in the ocean. This source is probably negligible in the Arctic spring and at the Dead Sea.
5. M. Hausmann and U. Platt, *J. Geophys. Res.* **99**, 399 (1994).
6. M. Tuckermann *et al.*, *Tellus* **49B**, 533 (1997).
7. K. Kreher, P. V. Johnston, S. W. Wood, B. Nardi, U. Platt, *Geophys. Res. Lett.* **24**, 3021 (1997).
8. A. Richter, F. Wittrock, M. Eisinger, J. P. Burrows, *ibid.* **25**, 2683 (1998).
9. T. Wagner and U. Platt, *Nature* **395**, 486 (1998).
10. U. Platt and J. Stutz, Eds., *HALOTROP Final Report* (University of Heidelberg, Heidelberg, 1998).
11. U. Platt and C. Janssen, *Faraday Discuss.* **100**, 175 (1995).
12. B. Alicke, K. Hebestreit, J. Stutz, U. Platt, *Nature*, in press.
13. T. M. Niemi, Z. Ben-Avraham, J. R. Gat, Eds., *The Dead Sea, The Lake and Its Setting*, vol. 36 of *Oxford Monographs on Geology and Geophysics* (Oxford Univ. Press, New York, 1997).
14. Dead Sea water is enriched in bromide by a factor of 70 relative to ocean water (0.07 g/liter$_{water}$ Br^- in standard mean ocean water, 5 g/liter$_{water}$ in Dead Sea water).
15. U. Platt and D. Perner, in *Optical and Laser Remote Sensing*, D. Killinger and A. Mooradien, Eds. (Springer-Verlag, New York, 1983), vol. 39 of *Springer Series in Optical Sciences*, pp. 95–105.
16. The DOAS instrument used at the Dead Sea consists of two parts. A receiving Newtonian telescope (f = 1.8 m, main mirror diameter 300 mm) was located in the van together with the spectrograph (0.5 m Czerny-Turner instrument, Spex 1870C, 600 g/mm) and a slotted disk spectral scanning device (*5, 15, 17, 25*) as detector. The xenon arc lamp (Osram XBO 450W/4) together with a transmitting telescope (f = 265 mm, diameter 300 mm) was placed on the rooftop of a hotel 3.75 km south of the receiver. Spectra were recorded in the wavelength interval from 324 to 349 nm with a resolution of 0.25 nm. For the wavelength calibration of the detector-spectrograph system, the mercury emission line at 334.15 nm was recorded frequently. Atmospheric spectra were recorded with a 30-min time resolution. Background spectra were recorded within 5 min after each atmospheric spectrum to correct for scattered light in the atmosphere. Each spectrum was high-pass filtered by dividing by a fitted seventh-degree polynomial. Using a least squares method (*18*), we evaluated each spectrum by fitting three trace gas reference spectra. Spectra of O_3 and NO_2 were recorded by inserting a quartz cell filled with the respective gas into the light path; the BrO spectrum was created by degrading the literature spectrum of Wahner *et al.* (*26*) to our instrument function, yielding a differential absorption coefficient of $\sigma' = 1.03\ (\pm 0.1) \times 10^{-17}$ cm^2 for the 339-nm band.
17. U. Platt, *Chem. Anal. Ser.* **127**, 27 (1994).
18. J. Stutz and U. Platt, *Appl. Opt.* **35**, 6041 (1996).
19. F. Ferlemann *et al.*, *Geophys. Res. Lett.* **25**, 3847 (1998).
20. D. Wagenbach *et al.*, *J. Geophys. Res.* **103**, 10961 (1998).
21. R. Vogt, P. J. Crutzen, R. Sander, *Nature* **383**, 327 (1996).
22. B. Finlayson-Pitts and S. N. Johnson, *Atmos. Environ.* **22**, 1107 (1988).
23. S.-M. Fan and D. J. Jacob, *Nature* **359**, 522 (1992).
24. M. Mozurkewich, *J. Geophys. Res.* **100**, 199 (1995).
25. F. Heintz, H. Flentje, R. Dubois, U. Platt, *ibid.* **101**, 891 (1996).
26. A. Wahner, A. R. Ravishankara, S. P. Sander, R. R. Friedl, *Chem. Phys. Lett.* **152**, 507 (1988).

1 October 1998; accepted 18 November 1998

Electrochemical Principles for Active Control of Liquids on Submillimeter Scales

Benedict S. Gallardo, Vinay K. Gupta,* Franklin D. Eagerton,
Lana I. Jong,† Vincent S. Craig, Rahul R. Shah,†
Nicholas L. Abbott†‡

Electrochemical methods were combined with redox-active surfactants to actively control the motions and positions of aqueous and organic liquids on millimeter and smaller scales. Surfactant species generated at one electrode and consumed at another were used to manipulate the magnitude and direction of spatial gradients in surface tension and guide droplets of organic liquids through simple fluidic networks. Solid microparticles could be transported across unconfined surfaces. Electrochemical control of the position of surface-active species within aqueous films of liquid supported on homogeneous surfaces was used to direct these films into periodic arrays of droplets with deterministic shapes and sizes.

The development of simple and general principles for the pumping and positioning of liquids on submillimeter scales will enable fabrication of microanalytical instrumentation that would make procedures such as blood chemistry analysis, flow cytometry, polymerase chain reactions, and DNA screening both rapid and inexpensive (*1*). Current methods used to pump liquids within networks of channels, or to position liquids within arrays, generally rely on electrokinetic phenomena driven by high voltages (several kilovolts) (*2*), mechanical syringes and actuators that are complicated to fabricate and too expensive to be disposable (*3*), or passive fluid phenomena such as capillary wetting (*4*). These methods are used to achieve largely serial manipulations of liquids (*3*) within permanent channels that direct the liquid motion (*2–4*). Here we report principles for the active control of liquids by the creation of gradients in surface pressure. In the same manner that changes in bulk solute concentration can lead to osmotic swelling (fluid transport), gradients in concentrations of molecules can lead to changes in surface tension that can be used to drive fluid motion. We created these gradients by using electrode surfaces to generate and consume surface-active species. This approach avoids the use of moving parts, uses low voltages (<1 V), permits vectorial transport and positioning of materials on unconfined surfaces, and can be applied to organic and aqueous liquids as well as solid microparticles. These methods make possible parallel manipulations of liq-

---

Department of Chemical Engineering and Materials Science, University of California, Davis, CA 95616, USA.

*Present address: Department of Chemical Engineering, University of Illinois, Urbana, IL 61801, USA.

†Present address: Department of Chemical Engineering, University of Wisconsin, Madison, WI 53706, USA.

‡To whom correspondence should be addressed. E-mail: abbott@engr.wisc.edu